

## Long Waves and Beach Profile Evolutions

H. Michallet, F. Grasso and E. Barthélemy

Laboratoire des Ecoulements Géophysiques et Industriels

(CNRS – UJF – INPG)

BP 53, 38041 Grenoble cedex 9, France

herve.michallet@hmg.inpg.fr



### ABSTRACT

MICHALLET, H., GRASSO, F. and BARTHÉLEMY, E., 2007. Long waves and beach profiles evolutions. *Journal of Coastal Research*, SI 50 (Proceedings of the 9th International Coastal Symposium), 221 – 225. Gold Coast, Australia, ISSN 0749.0208

Experiments were carried out in a flume 36 m long and 55 cm wide equipped with a piston wave generator. The sloping bottom consists of a loose material of low density ( $1190 \text{ kg m}^{-3}$ ) with a median diameter  $d_{50}=0.6 \text{ mm}$  in order that Shields and Rouse numbers are of the same magnitude as those of natural environments. Time and length scales ratios are roughly 1/3 and 1/10. Irregular waves were generated according to a JONSWAP spectrum. The waves were measured along the flume and bottom profiles were recorded in between repeated wave sequences. A wave climate (characterized by its peak frequency and root mean square wave height) was run for several tens of hours, so as to reach bottom equilibrium conditions.  $H_{\text{rms}}$  and infragravity mode amplitudes along the flume were obtained for transient and equilibrium bottom profiles. The long waves node positions and structure conform to model solutions of the linearized Saint-Venant equations. On the equilibrium bottom profile they are more energetic and the correlation between infragravity waves and the incident short wave envelope clearly indicate that they conform on both breaking point and bound long wave release mechanisms.

**ADDITIONAL INDEX WORDS:** *Irregular waves, Equilibrium beach profile, Infragravity waves*

### INTRODUCTION

Field measurements indicate that waves in the infragravity range play an important role on beach morphology. The generation of such long period waves can be explained by two different mechanisms. On one hand the breaking is thought to release bound long waves due to wave grouping (LONGUET-HIGGINS and STEWART, 1962). On the other hand wave grouping produces a break point and set-up oscillation that acts as a piston at the wave group period (SYMONDS et al., 1982). In both cases these incident long period waves reflect on the beach face, interfering with the incident waves to produce long period standing waves known as surf-beats. The strong correspondence in field experiments between long wave and morphological features length scales (AAGAARD and BRYAN, 2003), has suggested that long waves may generate off-shore bars. While strongly depending on the incident wave conditions (CERTAIN et al., 2005), these infragravity waves also play an important role on the swash process (MASSELINK et al., 2005). Nevertheless, descriptions of these long waves on real beaches are difficult due to the need of high spatial and temporal resolutions and tri-dimensional effects. Besides, wave climates and beach topographies are continuously changing in the real environment.

In a wave basin, WANG et al. (2002) performed velocity and concentration measurements over a beach that was formed by breaking irregular waves. A similar topography was obtained in a wave flume and included turbulent measurements in the surf zone suspension by HURTHER et al. (2007). Such laboratory experiments in wave tanks with beaches made of loose material are rare (DETTE et al., 2002). Most experimental studies were performed with a rigid bottom topography. JANSSEN et al. (2003) evaluated the long waves generation for a mild slope topography

moulded in sand with a smooth concrete surface. They concluded on a dominant mechanism of bound wave release. BALDOCK and HUNTLEY (2002) and BALDOCK et al. (2004) observed breaking forced waves for steeper uniform slopes and a barred beach profile.

The aim of the present paper is to investigate the characteristics of such surf-beats in small-scale mobile bed experiments and evaluate their relation to the bottom profile under controlled conditions.

### EXPERIMENTAL SET-UP

Experiments were carried out in a flume 36 m long and 55 cm wide equipped with a piston wave generator. The still water depth was 55.3 cm. The mean overall slope is approximately 1/40. The sloping bottom consists of a loose material (PolyMethyl MethAcrylate particles) of low density ( $1190 \text{ kg m}^{-3}$ ) with a median diameter  $d_{50}=0.6 \text{ mm}$ . In the experiments, the Froude number, the Shields number in the shoaling part and the Rouse number in the breaking zone (ratio of turbulent agitation to the settling velocity of the sediment) were of the same magnitude as those in natural environments. Time and length scales were roughly 1/3 and 1/10. Irregular waves were generated according to a JONSWAP spectrum (peak enhancement factor  $\gamma=3.3$ ). For each simulation, it is ensured that these waves conform to the expected spectrum and that they follow a Rayleigh distribution at 2 m downstream of the wave maker. Twelve wave gauges mounted on trolleys measured instantaneous water elevations over at least 30 minutes durations to obtain statistical convergence. Bottom profiles are recorded between wave series.

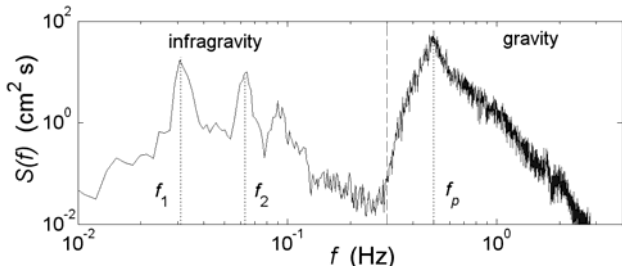


Figure 1. Surface elevation energy spectrum at  $x=2$  m in the flume on the equilibrium beach plotted in fig. 2d (---). On the right: “gravity” domain, corresponding to the generated JONSWAP spectrum. On the left: “infragravity” domain, generated by wave breaking. Wave parameters:  $H_{rms0}=7.5$  cm,  $f_p=0.5$  Hz,  $h_0=55.3$  cm. Two first modes infragravity frequency peaks  $f_1=0.031$  Hz and  $f_2=0.063$  Hz.

Spectral estimates  $S(f)$  were obtained from Fourier transforms of five 50 overlapping data segments, each comprising 32768 points sampled at 50 Hz. A wave spectrum measured at  $x = 2$  m has been plotted in Figure 1. Frequencies above  $3/5 \times f_p$ , correspond to the generated JONSWAP spectrum, representing the “gravity” domain. The generation of low frequency waves was clearly

visible in the power spectral density below  $3/5 \times f_p$  (this is the “infragravity” domain). A closer inspection of the low frequency range showed a broad peak at a frequency  $f_1$  around 0.03 Hz. Harmonics of this peak were also visible. The amplitude of the long wave motion was estimated within finite frequency bands of 0.02 Hz centered on peak frequencies as the square root of twice the sum of  $S(f)$ . The energy contained at various locations along the flume was estimated.

### LONG WAVES STRUCTURE

A wave climate characterized by its peak frequency ( $f_p=0.5$  Hz) and the root mean square wave height at 2 m downstream of the wave maker ( $H_{rms0}=7.5$  cm) was run for several tens of hours. Evolutions of  $H_{rms}$  and infragravity mode amplitudes along the flume are plotted in Figure 2 for two different bottom profiles. These (plotted in Figure 2d) correspond to two different stages. One is a transient stage characterized by a bar that travels onshore at about 1 m/h. This profile shows interesting similarity to the rigid bottom profile in the experiments of BALDOCK *et al.* (2004). The other profile is at equilibrium in the sense that there is no additional change (at plotting precision) over several hours. Note that the barred profile data is more scattered than the equilibrium profile data. The bottom changes between two sets of measurements are not entirely negligible in this case.

The infragravity wave energy is plotted in terms of significant amplitude in Figures 2b-c. The first mode amplitude is maximum

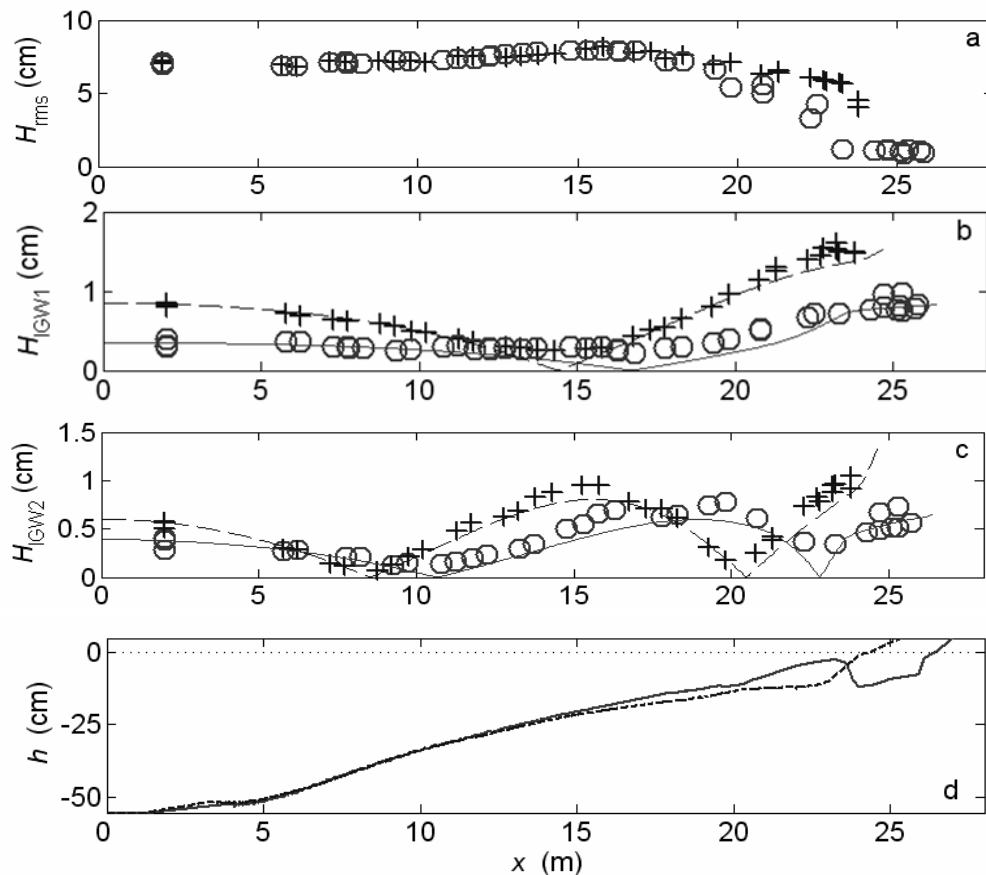


Figure 2. Wave and bottom characteristics along the flume axis for equilibrium profile (+) and transient profile (o): a) root mean square wave height, b) 1<sup>st</sup> mode infragravity rms wave height, c) 2<sup>nd</sup> mode infragravity rms wave height and d) equilibrium bottom profile (---) and transient bottom profile (—).

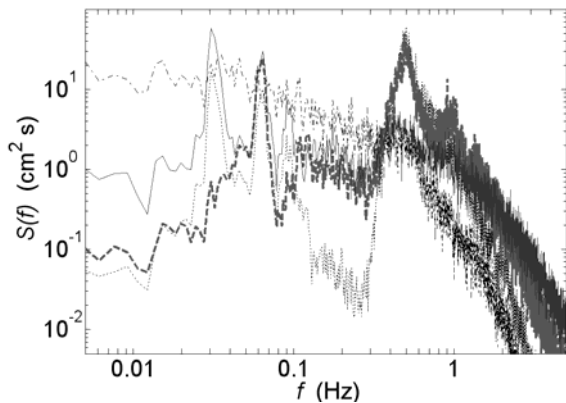


Figure 3. Total wave energy spectra at  $x = 2$  m (...),  $x = 15.3$  m (---),  $x = 23.3$  m (—) and spectrum of the short wave envelope at  $x = 2$  m (-.-); equilibrium bottom profile.

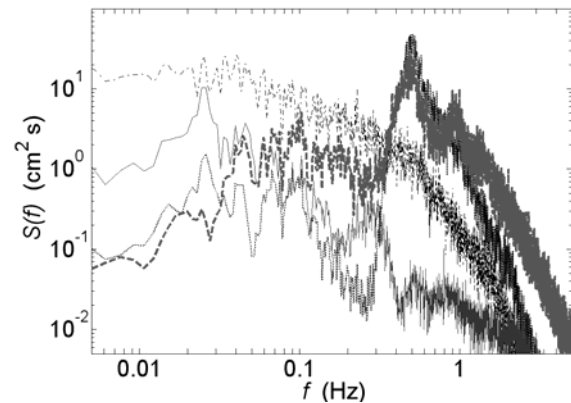


Figure 4. Total wave energy spectra at  $x = 2$  m (...),  $x = 16.8$  m (---),  $x = 25.8$  m (—) and spectrum of the short wave envelope at  $x = 2$  m (-.-); transient bottom profile.

at the berm, minimum close to  $x=15$  m and large again close to the wave maker. This indicates that a low frequency standing wave with a node somewhere around  $x=15$  m is generated in the flume. Despite the fact that the equilibrium profile is far from being a plane beach, the Wilson formula for a uninodal seiche in a rectangular flume with a uniform beach reported by DEAN and DALRYMPLE (1984, p.149) gives a very good estimate of  $f_1$  (i.e. 0.03 Hz). In addition, the data was compared with an analytical solution for a small amplitude free standing long wave of the linearized Saint-Venant equations (plotted in Figures 2b-c as a solid line for equilibrium profile and a dashed line for the transient profile). The solution yields with the modes frequencies, the nodal structure and the relative amplitudes as the amplitudes are fitted to the data at  $x=2$  m. The overall agreement of the nodal structure is good and the peak frequencies are remarkably well predicted (i.e.  $f_1=0.031$  Hz and  $f_2=0.063$  Hz for the equilibrium profile and  $f_1=0.024$  Hz and  $f_2=0.047$  Hz for the transient profile). The infragravity standing waves are always present whatever shape the bottom profiles have.

Our results in the barred case exhibit the same features, in terms of long wave amplitudes and node positions, as the results of BALDOCK et al. (2004). They concluded that a maximum long wave radiation occurs when the mean breakpoint closely coincides with the nodal point for the long wave on the barred beach. In our experiments, the long waves are more energetic on the equilibrium bottom profile for which the breaking point and first mode node position are several meters apart. Experiments performed for other wave conditions show that the long wave structure mainly depends on the beach morphology rather on the generated wave characteristics.

### WAVE SPECTRA

Surface elevation energy spectra for the two different topographies are plotted in Figures 3 and 4. They are presented for three positions along the flume that correspond to the deep region, the breaking region and close to shoreline. The location of the breaking region (maximum of  $H_{rms}$  in Figure 2a) is close to the node of the first mode (Figure 2b) and the anti-node of the second mode (Figure 2c). The spectra confirm that the energy in the infragravity domain is larger and the peaks more clearly defined in the case of the equilibrium profile. In the case of the transient profile, we may note that the energy in the gravity domain is very

low close to the shoreline. Indeed, the short waves have dissipated almost all their energy passing the bar, as indicated by the estimate of  $H_{rms}$  for  $x>23$  m in Figure 2a.

In addition, the spectrum of the short wave envelope, obtained via a Hilbert transform of the measured surface elevation data, is plotted in dashed-dotted line in Figures 3 and 4. This does not account for real energy in surface elevation but as energy possibly contained in the wave packets that could be released in the breaking region. It is important to emphasize that there is no dominant frequency in the wave grouping. This confirms that the frequency peaks of the infragravity waves depend on the beach profile only.

### CORRELATION WITH SHORT WAVE ENVELOPE

Figure 5 shows the cross-correlation between the short wave envelope in the constant depth region of the flume ( $x=2$  m) and the total low pass filtered surface motion ( $f<0.3$  Hz) at  $x=2$  m, in the breaking region and close to shoreline. There is a negative correlation for lags close to zero at  $x=2$  m. This corresponds to the locally forced incident bound long wave, which is out of phase with the short wave envelope (LONGUET-HIGGINS and STEWART, 1962). The lag is increasing and the correlation becomes stronger further shoreward as the bound wave shoals and represents a larger proportion of the total long wave energy (at  $\tau\approx 10$  s and  $x=15.3$  m). This bound wave is released in the shoaling and breaking and still negatively correlated to the wave envelope at lags  $\tau\approx 18$  s at  $x=2$  m and  $\tau\approx 20$  s at  $x=23.3$  m. On the other hand, a positive correlation is seen for  $\tau\approx 7$  s at  $x=15.3$  m. This corresponds to a dynamic setup generated by the breaking of the wave packets. The correlation becomes very strong at the shoreline ( $\tau\approx 13$  s). The long wave is reflected and propagates offshore as seen on the correlation signature for  $\tau\approx 21$  s at  $x=15.3$  m and  $\tau\approx 28$  s at  $x=2$  m. At larger lags, both negative and positive correlation peaks are still present but damped. This indicates that the long waves reflect on both ends of the flume but are not amplified. JANSSEN et al. (2003) concluded on a dominant mechanism of bound wave release, in their mild slopes laboratory experiments, while BALDOCK et al. (2004) observed breaking forced waves for stronger slopes. Both mechanisms are clearly observed in our case of an equilibrium beach profile.

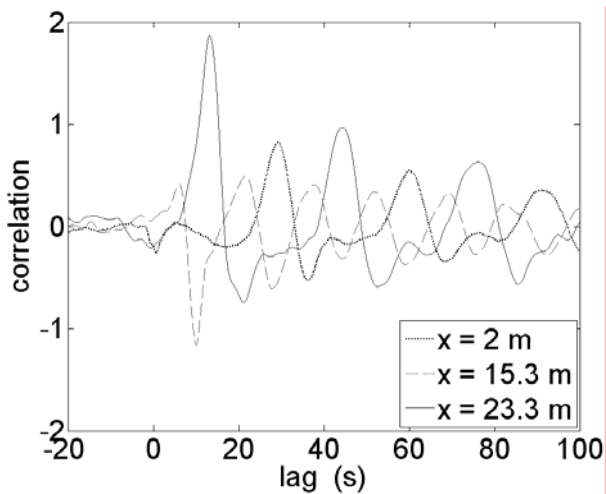


Figure 5. Cross-correlation between the infragravity waves and the short wave envelope at  $x=2$  m, equilibrium bottom profile.

To further understand the process, a large wave packet is considered. The first large waves travelling at the phase velocity produce an increase of the setup. The bound long wave propagates slower, at the group velocity. Once released, the free wave propagates at the phase velocity in both directions, onshore and offshore. The time travel of the free long wave from breaking region to shoreline and back is about the same as the one to the wave-maker and back (*i.e.* approximately 16 s). This lowers the mean water level and may enhance the breaking of the short waves at that time and thus maintains the process. This justifies the good agreement between first mode node and second mode anti-node positions (Figures 2b-c) in this very special equilibrium configuration.

For the transient bottom profile, the correlation picture shown in Figure 6 is in marked contrast. The correlation peaks at weaker values compared to the equilibrium case. The bound long wave signature is seen for  $\tau \approx 0$  s and  $\tau \approx 22$  s in the deep region and for  $\tau \approx 12$  s in the breaking region ( $x=16.8$  m) but not really at the shoreline ( $x=25.8$  m). More clearly the dynamic setup induces a stronger positive correlation for  $\tau \approx 8$  s at  $x=16.8$  m and  $\tau \approx 18$  s at  $x=25.8$  m. The break point mechanism is apparently dominant for this topography that is closer to BALDOCK *et al.* (2004) experiments. We also note that the long wave is partially reflected by the bar and the berm as indicated by the double peak for  $\tau \approx 27$  s and  $\tau \approx 38$  s at  $x=2$  m. This probably leads to the weak correlation for larger time lags ( $\tau > 60$  s). Bound wave release and breakpoint forcing do not reinforce the generation of the infragravity waves as for the equilibrium beach profile.

### BEGINNING OF THE WAVE SEQUENCE

The significant spectral peaks at the shoreline do not necessarily imply resonant amplification, since the incident short wave groups do not have a dominant frequency (as shown by the short waves envelope spectra in Figures 3 and 4). The generated wave packets are not necessarily in phase with the radiated long waves. In that sense, seiching is not really stationary in the flume. To illustrate this point, the beginning of the wave sequence is plotted in Figure 7. In Figure 7a, the short wave packets in the deep region are visible. They induce a modulation of the mean level close to shoreline. Resulting low frequency motions are shown in

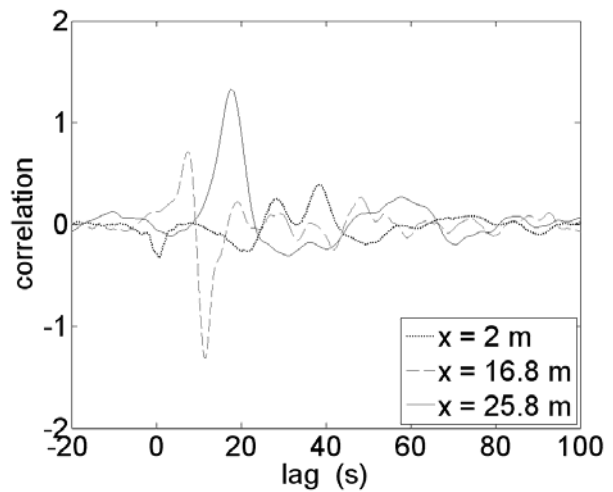


Figure 6. Cross-correlation between the infragravity waves and the short wave envelope at  $x=2$  m, transient bottom profile.

Figure 7b. The main period of about 32 s, corresponding to  $f_j$ , is sometimes observed. For instance, at  $x=23.8$  m, the peak for  $t \approx 34$  s is enhanced for  $t \approx 66$  s. In that case, a large wave packet has arrived in the breaking region in phase with the return of the generated long wave. This is not a general feature. The signature of a long wave is generally not seen after a couple of flume travel lengths. The main period of 32 s is not visible in the infragravity wave signal corresponding to the deep region for  $t > 130$  s in Figure 7b. In that sense, amplification in the long wave generation process is not noted.

### CONCLUSIONS

The experiments show that the long wave structure strongly depends on the beach morphology rather than on the generated short wave characteristics. In particular, the infragravity waves are more energetic on the equilibrium bottom profile compared to the transient barred profile. The nodal structure of the infragravity waves is determined by the beach shape that is, mainly the distance between the breaking point and the shoreline.

The correlation between the infragravity waves and the incident short wave envelope indicate that the infragravity waves generation conform to both breaking point and bound long wave release mechanisms.

It is suggested that the beach topography evolves as to reinforce both the bound long wave release and the dynamic setup generation. At equilibrium, the distance between breaking and shoreline is such that the return of the free wave lowers the water level and energizes the breaking of wave packets. These experiments yield new results for a deeper understanding of the link between infragravity waves and beach dynamics.

### LITERATURE CITED

- AAGAARD, T. and BRYAN, K.R., 2003. Observations of infragravity wave frequency selection, *Cont. Shelf Res.*, 23, 1019-1034.  
 BALDOCK, T.E.; O'HARE, T.J. and HUNTLEY, D.A., 2004. Long wave forcing on a barred beach, *J. Fluid Mech.*, 503, 321-343.  
 BALDOCK, T.E. and HUNTLEY, D.A., 2002. Long wave forcing by the breaking of random gravity waves on a beach, *Proc. R. Soc. Lond.*, A 458, 2177-2201.

- CERTAIN, R.; MEULÉ, S.; REY, V. and PINAZO, C., 2005. Wave transformation on a microtidal barred beach (Sète, France), *J. Marine Systems*, 38, 19-34.
- DEAN, R.G. and DALRYMPLE, R.A., 1984. *Water Wave Mechanics for Engineers and Scientists*, World Scientific.
- DETTE, H.H.; LARSON, M.; MURPHY, J.; NEWE, J.; PETERS, K.; RENIERS, A. and STEETZEL, H., 2002. Application of prototype flume tests for beach nourishment. *Coastal Eng.*, 47, 137-177.
- HURTHUR, D.; MICHALLET, H. and GONDRAN, X., 2007. Turbulent measurements in the surf zone suspension. *Journal of Coastal Research*, S150.
- JANSSEN, T.T.; BATTJES, J.A. and VAN DONGEREN, A.R., 2003. Observation of long waves induced by short wave groups, *J. Geophys. Res.*, 108, 3252-3264.
- LONGUET-HIGGINS, M.S. and STEWART, R.W., 1962. Radiation stress and mass transport in gravity waves, with application to 'surf-beats', *J. Fluid Mech.*, 13, 481-504.
- MASSELINK, G.; EVANS, D.; HUGHES, M.G. and RUSSEL, P., 2005. Suspended sediment transport in the swash zone of a dissipative beach, *Marine Geol.*, 216, 169-189.
- SYMONDS, G.; HUNTLEY, D.A. and BOWEN, A.J., 1982. Two dimensional surf beat: long wave generation by a time-varying break point, *J. Geophys. Res.*, 87(C1), 492-498.
- WANG, P.; EBERSOLE, B.A.; SMITH, E.R. and JOHNSON, B.D., 2002. Temporal and spatial variations of surf-zone currents and suspended sediment concentration, *Coastal Eng.*, 46, 175-211.

### ACKNOWLEDGEMENT

This work has been partially funded by the CNRS-INSU PATOM. The technical support of J.-M. Barnoud is gratefully acknowledged.

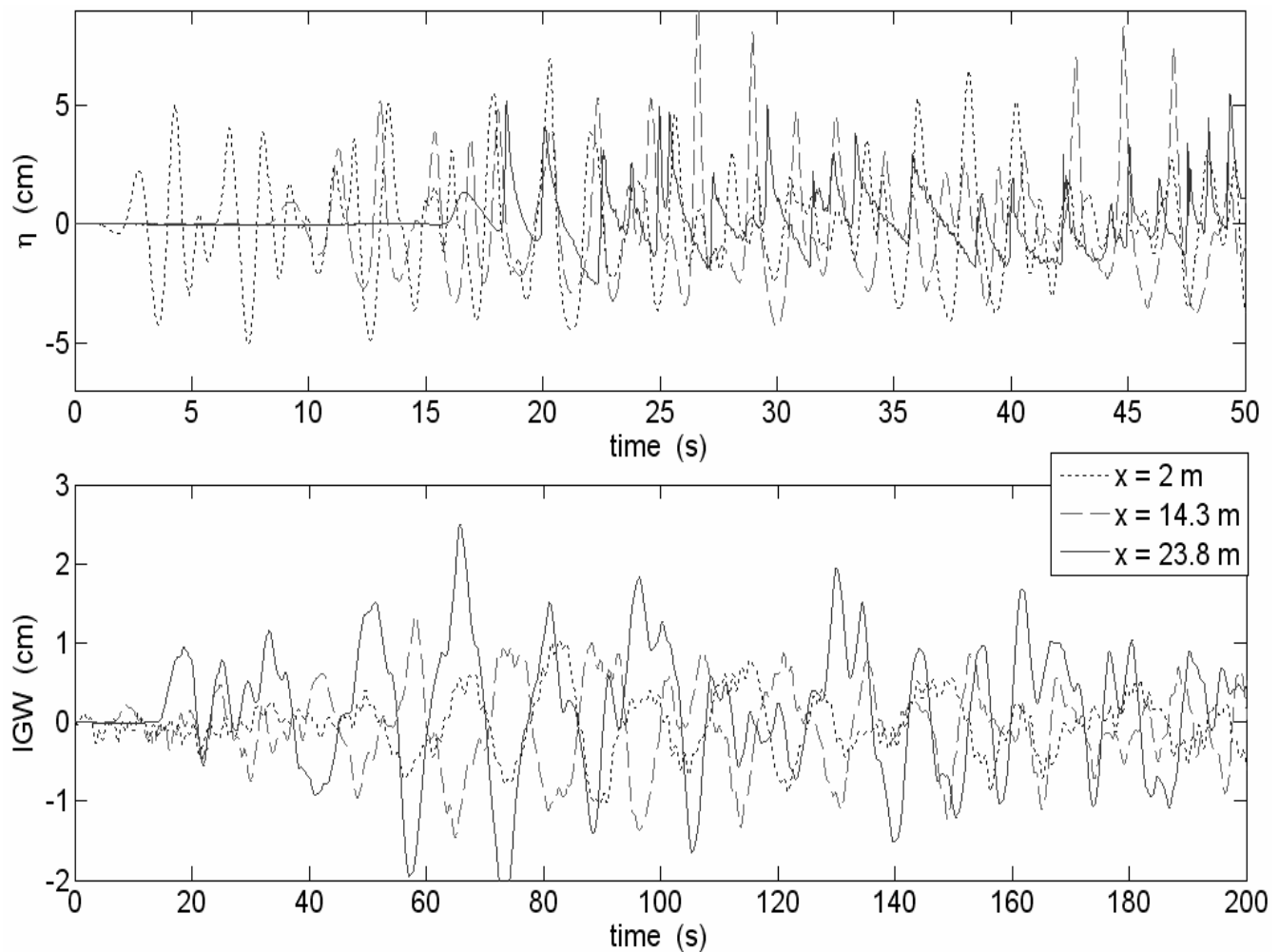


Figure 7. Surface elevations (a) and infragravity waves (b) in the deep, breaking and shoreline regions for the equilibrium bottom profile.